Journal of CO2 Utilization 83 (2024) 102821

Contents lists available at ScienceDirect

Journal of CO2 Utilization

journal homepage: www.elsevier.com/locate/jcou

Improving the early reactivity of activated basic oxygen furnace slag – The influence of particle fineness and grinding aids

J.C.O. Zepper [a,b,*], S. de Bruin [a], X. Ling [a], K. Schollbach [a], S.R. van der Laan [a,c], H.J.H. Brouwers [a]

[a] Department of the Built Environment, Eindhoven University of Technology, P. O. Box 513, Eindhoven, 5600MB, The Netherlands
[b] Tata Steel, TEC CoE SMC, P.O. Box 10000, IJmuiden 1970CA, The Netherlands
[c] Tata Steel, RDT MSC, P.O. Box 10000, IJmuiden 1970CA, The Netherlands

ARTICLE INFO

Keywords:
Basic oxygen furnace slag
Activation
Grinding aids
Reactivity
Particle fineness

ABSTRACT

Basic oxygen furnace slag (BOF slag), also known as Linz-Donauwitz slag, is an industrially by-product of the steel industry and produced during the converter process. In this research we have investigated the effect of grinding aids and particle fineness on the hydration of potassium citrate activated BOF slag. It was investigated the effects of five different grinding aids on the grindability and hydration of activated BOF slag in laboratory batch milling experiments. The grinding aids generally improve the grindability of BOF slag and therefore increase the particle fineness of BOF slag. This had the consequence that the hydration of activated BOF slag was improved. Only one grinding aid, triethanolamine (TEA) also improved the hydration of BOF slag besides providing higher particle fineness. The combination of the higher particle fineness and additional effect of TEA on the hydration improved the compressive strength to 60 and 78 MPa of activated BOF slag. An additional important of this research is that the hydration of BOF slag is significantly more sensitive on particle fineness compared to ordinary Portland cement.

1. Introduction

It is well known that the cement and concrete industry is a major contributor to global CO_2 emissions. Approximately 6 – 7 wt% of global CO_2 are produced during the production of ordinary Portland cement (OPC). Approximately 850 kg CO_2 per tonne OPC clinker is emitted [1]. The main part of these emissions (~90%) are produced during the clinkering process [2]. One possibility to reduce CO_2 emissions is to reduce the usage OPC and increase the usage of supplementary cementitious materials (SCM) like ground granulated blast furnace slag (GGBFS), fly ash or other emerging SCMs [3]. The second possibility is to use OPC free alternative binders with a low CO_2 footprint [4,5]. One of those alternatives as an OPC free binder could be basic oxygen furnace (BOF) slag [6].

BOF slag, also known as Linz-Donawitz slag, is a by-product of the steel industry and from the converter process [7,8]. BOF slag is produced in large amounts. Per ton steel about 100 kg of BOF slag is produced with an annual amount of more than 100 Mt [9] worldwide. The largest share of BOF slag is either used in low-end applications such as road fill or is landfilled [10,11]. A suitable application for BOF slag has been suggested in building materials and has been intensively researched [7, 12–15]. The interest is based on the large amounts available and a mineralogical composition comparable to, which is evidenced by the presence of phases such as C_2S, $C_2(A,F)$ and C_3S [7,11,13,16]. More importantly there are no clinkering CO_2 emissions attached to BOF slag because they are attached to the steel products. Only CO_2 emissions of energy that is consumed during the milling process need to be considered.

However, unlike OPC, BOF slag lacks the large amounts of C_3S and shows therefore only very low hydraulic reactivity [17–19]. Moreover, BOF slag is not suitable as a supplementary cementitious material (SCM) since it is reported to lower the hydraulic reactivity of OPC by reducing the pH in the pore solution and preventing the precipitation of portlandite and subsequently delaying the formation of CSH [20,21] and only low amounts (10 – 20 wt%) of BOF slag are recommended for SCM with OPC [15]. Therefore, several other studies aimed to activate BOF slag as the stand-alone binder to serve as a cementitious system through hydrothermal [22], thermal [23], chemical [19,24–26] and carbonation

* Correspondence to: Department of the Built Environment, Eindhoven University of Technology, P. O. Box. 513, Eindhoven, MB 5600, the Netherlands.
E-mail address: j.c.o.zepper@tue.nl (J.C.O. Zepper).

https://doi.org/10.1016/j.jcou.2024.102821
Received 8 April 2024; Received in revised form 15 May 2024; Accepted 22 May 2024
Available online 24 May 2024

activation [27]. Some attention has been paid in these lone binder systems on the importance of particle fineness [28–31]. For example, Franco Santos et al. [31] reported that by reducing the D50 from 56 to 16 μm the cumulative heat determined by isothermal calorimetry, which develops from the BOF slag reacting with water, more than doubles in the first 90 h of hydration. Liu and Li [28] reported a similar observation. Within their study the specific surface area (SSA) was increased from 3890 to 6350 cm^2/g by additional grinding, which had the consequence that the cumulative heat determined by isothermal calorimetry also nearly doubled. The importance of particle fineness has also been reported for the reactivity of C_2S [32], which is the phase that is most present in BOF slag [33,34]. Other studies have tried to promote reactivity by mechanical activation through milling and focused on the application of BOF slag as SCM [35] or for carbonation curing [36]. Additionally, the study of Xi et al. [30] investigated the use of several grinding aids in order to reduce the particle size of the BOF slag binder. Among the applied grinding aids were for example glycerol, triethanolamine and calcium lignosulfate. The addition of grinding aid was 0.05 wt% per mass of the BOF slag. The reported results are that the grindability of BOF slag was significantly improved, when a grinding aid was applied. The improved grindability was illustrated in the SSA results, whereas milled BOF slag with a grinding aid showed a 30% higher SSA compared to the milled BOF slag without grinding aid. Generally, grinding aids serve as surface energy reducers during the grinding operation of solid particles [37]. In the cement industry, grinding aids have been applied since the late 1930s and do not only produce finer powders at the same energy input during the grinding operation but also have an effect on the hydration kinetics of cementitious powders [38].

To improve the cementitious properties of chemically activated BOF slag, it was decided to further investigate the impact of fineness on the early hydration of tri potassium citrate monohydrate (K3CitH) BOF slag (7 and 28 days). For that, different grinding aids were used in batch grinding of BOF slag using a high impact disc mill. The resulting particle fineness and the effect on the early hydration of a pure BOF slag binder activated by 1 wt% K3CitH were tested. The choice of K3CitH was made based on the promising results with BOF slag, which was shown by Kaja et al. [24]. The decision regarding 1 wt% addition was made based on the explanation that higher concentrations (> 1 wt%) would indeed promote the early hydration but would harm the later hydration of especially C_2S [24]. Moreover, higher concentrations K3CitH would probably be not economically interesting for cement producers. BOF slag samples have been milled with 5 different grinding aids for 10, 20, 30 min and compared to a sample without use of grinding aid as reference. So a total of 18 samples was investigated for their particle size distribution (PSD) determined by laser diffraction PSD and specific surface area determined by Blaine and Brunauer-Emmett-Teller surface area analysis (BET). The early hydration was investigated by isothermal calorimetry for 72 h. 7 and 28 days BOF slag pastes were evaluated by thermogravimetric analysis (TGA), Rietveld quantitative phase analysis (RQPA) and compressive strength of the pastes prepared at w/b of 0.16.

The ultimate aim is to understand the impact of particle fineness on the hydration and mechanical properties of K3CitH activated BOF slag. This will help in the further development of cementless BOF slag based binder.

2. Raw materials and methodology

2.1. Materials

2.1.1. BOF slag

The investigated BOF slag was obtained from Tata Steel Netherlands, after metal recovery treatment at the steel plant the BOF slag had the initial size of 0 – 250 mm. The BOF slag was subsequently crushed to below 5.6 mm and 50 kg was split with a splitter into batches of 1 kg ± 50 g in order to assure that the initial PSD is the same for all batches and does not influence the grinding results.

2.1.2. Grinding aids

Three traditional grinding aids were chosen, which were oleic acid or OA (Acros Organics, technical grade), triethanolamine or TEA (VWR Chemicals, technical grade) and glycerol or GL (Acros Organics, technical grade). Additionally, it was chosen to dissolve K3CitH in demineralized water to reach a concentration 4 mol/L or in glycerol (1 mol/L), the resulting solution was also used as grinding aid with MPW and MPG, respectively. All grinding aids have been applied by adding 500 mg per 1 kg of BOF slag prior to the grinding operation.

2.2. Material preparation

2.2.1. Grinding operation

1 kg of BOF slag was ground with or without the addition of 0.5 g of grinding aid. Ground BOF slag samples were derived by batch grinding in a Retch RS 300 XL discmill for 10, 20 and 30 min. This way a total of 18 samples were produced.

2.2.2. Paste

BOF slag pastes were prepared by using a w/b of 0.16. Prior to the mixing operation 1 wt% of K3CitH was dissolved in the water used for the paste mix. BOF slag powder and water were mixed in a mixing bowl with an electric mixer. The mixing procedure was 1 min low speed mixing (140 rotation and 62 planetary movement) 1.5 min of hand mixing, 1 min high speed mixing (285 rpm rotation and 125 planetary movement), 1.5 min of hand mixing and 1 min of high speed mixing. After testing the spread flow, the paste was returned into the mixing bowl and mixed again at high speed mixing for 30 s. The pastes were subsequently transferred into steel moulds with dimensions of 4*4*4 cm^3. The moulds with BOF slag paste were wrapped in cling film and stored for 1 day at 20 °C. After 1 day curing, sample cubes were demoulded and placed in water for an additional 6 or 27 days, so the cumulative curing time of 7 or 28 days, respectively.

Additional paste samples were prepared for TGA and RQPA pouring by 15–30 g fresh paste into a 50 ml plastic sample containers. After 24 h, the sample containers were filled up with water to reproduce the curing conditions of the paste cubes. After the desired curing time (i.e. 7 d or 28 d) samples were recovered and hydration was stopped by the di-solvent exchange method as described in [39].

2.3. Analytical methods

An experimental plan was devised (Table 1), for experimental tests. This experimental plan balances work load and the number of observations required to understand the BOF slag early reactive and hardening process with different grinding aids in the activator system of K3CitH.

PSD of ground powder samples was determined with laser diffraction particle size (LD-PSD) analysis using a Malvern Mastersizer 2000 equipped with a Hydro 2000S wet dispersion unit. All samples were dispersed in isopropanol. Prior to the laser diffraction analysis ultrasound treatment within the Mastersizer 2000 was applied for 1 min to decrease agglomeration of particles. The SSA_{Blaine} was determined according to standard EN 196–6. The BET analysis was performed on a Micromeritics Tristar 3000. Prior to the analysis the samples were degassed at 120 °C with a Micromeritics Flow Prep 060 LB. Each sample was analysed three times and averages are reported for SSA_{BET}.

The chemical composition of the IBOFS (Table 2) is determined by the combination of X-ray fluorescence analysis (XRF) bead analysis and Fe redox titration method. Prior to the XRF analysis LOI is determined and to remove any volatiles present in the sample by heating the sample material to 1000 °C. The fused bead is produced using lithium borate ($Li_2B_4O_7$:$LiBO_2$ = 65:35) in weight proportions of sample to borate 1:10. The fused bead is subsequently analysed on a PANalytical Axios. BOF slag contains multiple Fe species (Fe^0, Fe^{2+} and Fe^{3+}). In order to determine the different Fe species quantitatively the Fe redox titration

Table 1
Overview of the applied methodology in this study, n.d. stands for not determined. IBOFS refers to the initial BOF slag, R refers to the milled material without the application of grinding aids, OA refers to the milled material with oleic acid as grinding aid, TEA refers to the material with triethanolamine as grinding aid, MPW refers to the grinding aid that has been produced by dissolving 3KCitH in demineralized water to reach a concentration of 4 mol/L, GL refers to the material with glycerol as grinding aid, MPG refers to the grinding aid that has been produced by dissolving K3CitH in glycerol to reach a concentration of 1 mol/L and the numbers 10, 20 and 30 after the grinding aid abbreviation refer to applied milling time of 10, 20 and 30 min milling, respectively.

Sample	XRF	LD-PSD	Blaine	BET	Calorimetry	TGA	RQPA	Spread	Compr. Strength
IBOFS	√	n.d.	n.d.	n.d.	n.d.	n.d	√	n.d.	n.d.
R10	n.d.	√	√	√	√	7 and 28 d	7 and 28 d	√	7 d
R20	n.d.	√	√	√	√	7 and 28 d	7 and 28 d	√	7 d
R30	n.d.	√	√	√	√	7 and 28 d	7 and 28 d	√	7 and 28 d
OA10	n.d.	√	√	√	√	7 and 28 d	n.d.	√	7 d
OA20	n.d.	√	√	√	√	7 and 28 d	n.d.	√	7 d
OA30	n.d.	√	√	√	√	7 and 28 d	7 and 28 d	√	7 and 28 d
TEA10	n.d.	√	√	√	√	7 and 28 d	n.d.	√	7 d
TEA20	n.d.	√	√	√	√	7 and 28 d	n.d.	√	7 d
TEA30	n.d.	√	√	√	√	7 and 28 d	7 and 28 d	√	7 and 28 d
MPW10	n.d.	√	√	√	√	7 and 28 d	n.d.	√	7 d
MPW20	n.d.	√	√	√	√	7 and 28 d	n.d.	√	7 d
MPW30	n.d.	√	√	√	√	7 and 28 d	7 and 28 d	√	7 and 28 d
GL10	n.d.	√	√	√	√	7 and 28 d	n.d.	√	7 d
GL20	n.d.	√	√	√	√	7 and 28 d	n.d.	√	7 d
GL30	n.d.	√	√	√	√	7 and 28 d	7 and 28 d	√	7 and 28 d
MPG10	n.d.	√	√	√	√	7 and 28 d	n.d.	√	7 d
MPG20	n.d.	√	√	√	√	7 and 28 d	n.d.	√	7 d
MPG30	n.d.	√	√	√	√	7 and 28 d	7 and 28 d	√	7 and 28 d

Table 2
Chemical analysis results combined from XRF and Fe redox titration of the raw BOF slag (IBOFS). [d] denotes determined by Fe redox titration method (FeO^d and metallic Fe^d) and [c] denotes that it is recalculated from the XRF results for Fe total and subtracted from Fe^{2+} and Fe^0.

Sample ID	Al_2O_3	CaO	Cr_2O_3	$Fe_2O_3^c$	FeO^d	Met. Fe^d	MgO	MnO	P_2O_5	SiO_2	TiO_2	V_2O_5	Others	Fe total	LOI
IBOFS	2.0	40.9	0.3	13.2	11.5	0.9	7.8	4.9	1.7	14.1	1.4	1.0	0.1	19.1	-0.9

method was performed according to ISO 5416–2006 and ISO 9035:1989. The quantities of Fe^0 (i.e. metallic Fe) and Fe^{2+} (i.e. FeO) are used to calculate Fe^{3+} (i.e. Fe_2O_3).

Isothermal calorimetry (TAM Air, Thermometric) was performed on pastes with the mixing proportions of the moulded paste samples. BOF slag pastes were mixed ex-situ for 1 min prior to inserting the glass vials with the pastes into the calorimeter. The cumulative heat was derived by integrating the thermal power curve between 30 min and 72 h.

The loss of volatiles was studied with thermogravimetric analysis (TGA) on a Jupiter STA 449 F1 Netzsch instrument on hydration stopped paste samples cured in plastic containers. 60 – 80 mg of sample material was analysed under nitrogen atmosphere by heating to 1000 °C at a heat rate of 10 °C/min.

The sample preparation for the X-ray diffraction measurements was performed in the following steps: 1) 3.6 g of sample material was weighed in together with 0.4 g of metallic Si as internal standard, 2) weighed powder was ground together with 7 ml of cyclohexane added as cooling agent to analytical fineness (D50 $<$ 5 μm) by using a Retsch McCrone micronizer, 3) after milling the sample was recovered and dried for 5 min to evaporate the cyclohexane in a furnace at 65 °C. 4) analytical fine powder was back-loaded on a metal sample holder designed for X-ray diffraction measurement.

The X-ray diffraction patterns of the initial BOF slag and 28 d hydrated paste samples were taken by Bruker D8 X-ray diffractometer equipped with a Co anode and a LynxEye detector and a fixed divergence slit of 0.5° and primary and secondary collimeter of 2.5°. The X-ray diffraction patterns of the 7 d hydrated paste samples were taken by Malvern PANAlytical XpertPro with a Co anode with a Pixel 3D detector and a fixed divergence slit of 0.5∘ and 0.04 rad soller. The 2Theta range was for all measurements from 10 to 120°. RQPA performed on the X-ray diffraction patterns used the same strategy as reported in [22].

The compressive strength of pastes after was tested on 4*4*4 cm^3 cubes according to EN 196–1 with three replicates for each sample. After mixing, spread flow was tested using a similar mould used in EN 1015–3. The spread flow was tested without jolting operation, because the pastes showed significant differences in paste consistency, meaning that pastes derived from coarser powder showed low viscosity that it would flow of the jolting table if jolting would have been applied whereas the paste samples derived from the finest powders were very viscous. Therefore spread flow analysis was performed on a glass plate without jolting application.

2.4. Incorporation of available data from the literature for BOF slag binders

The data generated in this study was compared to studies that focused on the application of BOF slag as a stand-alone standing cementitious binder and where particle fineness was determined either by LD-PSD or Blaine method. Only data from the literature were included that either studied pure BOF slag [28,31], activated BOF slag [24–26,40–42] or hot stage modified BOF slag (i.e. Al_2O_3 addition) [43]. The data where BOF slag serves as an SCM together with a cement [44,45] or is a component in alkali activation with ground granulated blast furnace slag (GGBFS) or fly ash (FA) like in [46,47] were excluded. Also, it is emphasized here that this study specifically focuses on BOF slag, which is one type of steel slag among other types of steel slag such as electric arc furnace slag, ladle furnace slag, casting slag and slobbing slag, which all have different properties. The rationale to also include available data from literature was: i) to show how the hydration of BOF slag dependents on particle fineness, ii) to illustrate how other factors (i.e. different chemical and phase composition, hot stage modification, grinding methodology and activator type may influence the hydration kinetics of BOF slag and iii) to summarize the available data from the literature. However, the outcomes of the different analytical methods strictly are not comparable because of differences in the nature of the BOF slag, the material preparation and analytical methodology (e.g. alteration degree, w/b or temperature settings in the isothermal calorimetry experiments) [39]. Also other factors that may influence the

BOF slag properties and hence the hydration kinetics of BOF slag, which are not always reported such as carbonation during storage [48], different types BOF slag handling and cooling methodologies [49–51].

3. Results and discussion

3.1. Particle size distribution and specific surface area

Table 3 reports the results of LD-PSD, Blaine and BET for all 18 samples The increase in grinding time for the samples without the addition of a grinding aid (R10, R20 and R30) has the effect that D10, D50, D90 are reduced and all SSAs are increased, except for the SSA_{BET} of R20. The amount of larger particles is reduced at longer milling times which is depicted by the significant decrease of D50 and D90, which are reduced for R30 by 34% and 40%, respectively compared to R10. In comparison D10 of R30 is only 85% in size compared to D10 in R10. The grinding aids TEA and MPW show a comparable behaviour as the R-sample set with increasing grinding time decreasing D10, D50, D90, SSA_{PSD} and SSA_{Blaine} with increasing grinding time For example TEA30 has 43% and 37% lower D50 and D90, respectively compared to TEA10 whereas D10 is only reduced for 10%. In contrast, the grinding aids OA, GL and MPG show a different behaviour. The grinding is the most efficient regarding increase in SSA and decrease in PSD in the first 20 min. The D50 OA20 and GL20 are decreased significantly by 30% and 39%, respectively. Additionally, SSA_{Blaine} is increased for OA20 and GL20 by 79% and 101%, respectively. Furthermore, the results show that for 30 min grinding the D50 and SAA_{Blaine} and for these grinding aids do not significantly increase or decrease, respectively. For example the SSA_{Blaine} and D50 of OA and GL after 20 min and 30 min are not changed substantially.

The efficiency of the grinding aids are evaluated based on their efficiency achieving finer particles. Usually, the efficiency of a grinding aid is evaluated using the parameter Φ_{GA} using Eq. 1 [52]:

$$\Phi_{GA} = \frac{SSA_{m,GA}}{SSA_{m,ref}} \quad (1)$$

Whereas $SSA_{m,GA}$ and $SSA_{m,ref}$ are the specific surface areas of the product with grinding aid and of the reference without grinding aid, respectively, under identical grinding conditions (i.e equal grinding time). $\Phi_{GA,method,time}$ are determined for all methods and a mean value ($\Phi_{GA,mean,time}$) from all SSA methods. Also the overall grinding aid efficiency is calculated as a mean value per grinding for the three grinding times (Table 4; $\Phi_{GA,overall\ mean}$). The total mean $\Phi_{GA,overall\ mean}$ is 1.17, which means that grindability of BOF slag is improved by 17% by using some sort of grinding aid. Based on this averaging, TEA seems to perform the best as a grinding aid with $\Phi_{TEA,overall\ mean}$ of 1.3, whereas grinding aids MPW and MPG perform the worst with $\Phi_{GA,overall\ mean}$ of 1.05 and 1.1, respectively. However, all grinding aids help to generate an increased fineness although this does not hold-up for some grinding aids (e.g. MPW) after only 10 min of grinding.

Table 4
Mean grinding aid efficiency Φ_{GA} for each grinding aid, grinding time (i.e. 10, 20 and 30 min) and SSA method (i.e. BET, Blaine and LD-PSD).

Grinding Aid	$\Phi_{GA,overall\ mean}$
OA	1.19
TEA	1.30
MPW	1.05
GL	1.23
MPG	1.10

It is important to briefly discuss what kind of SSA is most important to a cementitious system and which correlates the best to the reactivity of binders and SCMs. It has been reported that regarding physical properties the fineness or specific surface area is the most controlling factor on the reactivity and ultimately strength of a cementitious binder (i.e. OPC or alkali activated binder) or SCM [17,53–55]. So the ultimate goal would be to determine the reactivity of activated BOF slag and eventually the mechanical properties (i.e. workability/spread flow and mechanical strength of pastes/mortars/concrete). The big question however is which method for determining the particle fineness or SSA gives the best prediction of material behaviour as binder or SCMs. Often research studies only focus on one method rather than multiple methods to relate particle fineness of the binder with the behaviour during hydration. Moreover, physical particle characteristics (i.e. fineness or shape) might dictate which characterization method gives the best prediction of the behaviour during hydration [56,57]. As for BOF slag, the studied particle fineness determined as cementitious material by the Blaine method is usually comparable to that of OPC (2500 – 6000 g/cm^2 SSA_{Blaine}) and usually lower than that of blast furnace slag (GGBFS) or calcined clays (> 5000 g/cm^2 SSA_{Blaine}) [28,29,55,56,58], which would suggest that methods determining the SSA of cement would also apply to BOF slag. Since BOF slag is, like OPC clinker and unlike fly ash, a cohesive and crystalline material BET analysis could also be used to relate the reactivity to the SSA_{BET}.

Fig. 1 illustrates the correlation between SSA of the different methods used to determine particle fineness. Best correlations for the sample suite are observed between SSA_{BET} – SSA_{PSD} and SSA_{Blaine}-$D50_{PSD}$ with and R^2 of 0.84 (Fig. 1 C and D). The lower correlation between SSA_{Blaine} - SSA_{BET} ($R^2 = 0.76$, Fig. 1 A) may be attributed to the

Table 3
Results of LD-PSD, Blaine and BET analysis and the respective calculated grinding aid efficiency Φ_{GA}, calculated with Eq. 1 and with n.a. standing for not applicable.

Sample	D10 (μm)	D50 (μm)	D90 (μm)	SSA_{PSD} (cm^2/g)	$\Phi_{GA,SSA\text{-}PSD}$	SSA_{Blaine} (cm^2/g)	$\Phi_{GA,Blaine}$	SSA_{BET} (m^2/g)	$\Phi_{GA,BET}$	$\Phi_{GA,mean,time}$
R10	2.54	14.22	64.96	2940	n.a.	2750	n.a.	1.06	n.a.	n.a.
R20	2.27	11.89	48.16	3280	n.a.	3580	n.a.	1.06	n.a.	n.a.
R30	2.15	9.41	38.71	3740	n.a.	4210	n.a.	1.80	n.a.	n.a.
OA10	2.75	13.52	58.18	2770	0.94	2620	0.95	1.17	1.10	1.00
OA20	1.84	8.40	40.20	4100	1.25	4680	1.31	1.92	1.80	1.45
OA30	2.09	8.46	40.70	3910	1.05	4780	1.14	2.03	1.13	1.10
TEA10	1.68	13.73	60.86	3670	1.25	3810	1.39	1.70	1.59	1.41
TEA20	1.88	11.16	49.78	3750	1.14	3970	1.11	1.72	1.62	1.29
TEA30	1.51	7.80	38.43	4640	1.24	4570	1.09	2.28	1.27	1.20
MPW10	2.87	18.52	129.89	2540	0.86	2310	0.84	1.05	0.99	0.90
MPW20	2.64	10.85	58.07	3220	0.98	3900	1.09	1.60	1.51	1.19
MPW30	1.91	8.70	42.62	4050	1.08	4290	1.02	1.91	1.06	1.06
GL10	2.34	16.14	81.29	2980	1.01	2520	0.92	1.20	1.13	1.02
GL20	2.25	9.85	46.99	3550	1.08	5070	1.42	2.02	1.90	1.47
GL30	1.83	8.05	38.48	4300	1.15	5190	1.23	2.24	1.24	1.21
MPG10	2.45	14.96	68.58	2990	1.02	2610	0.95	1.19	1.12	1.03
MPG20	2.30	10.60	46.53	3510	1.07	4200	1.17	1.30	1.22	1.15
MPG30	1.69	8.34	39.23	4410	1.18	4240	1.01	2.16	1.20	1.13

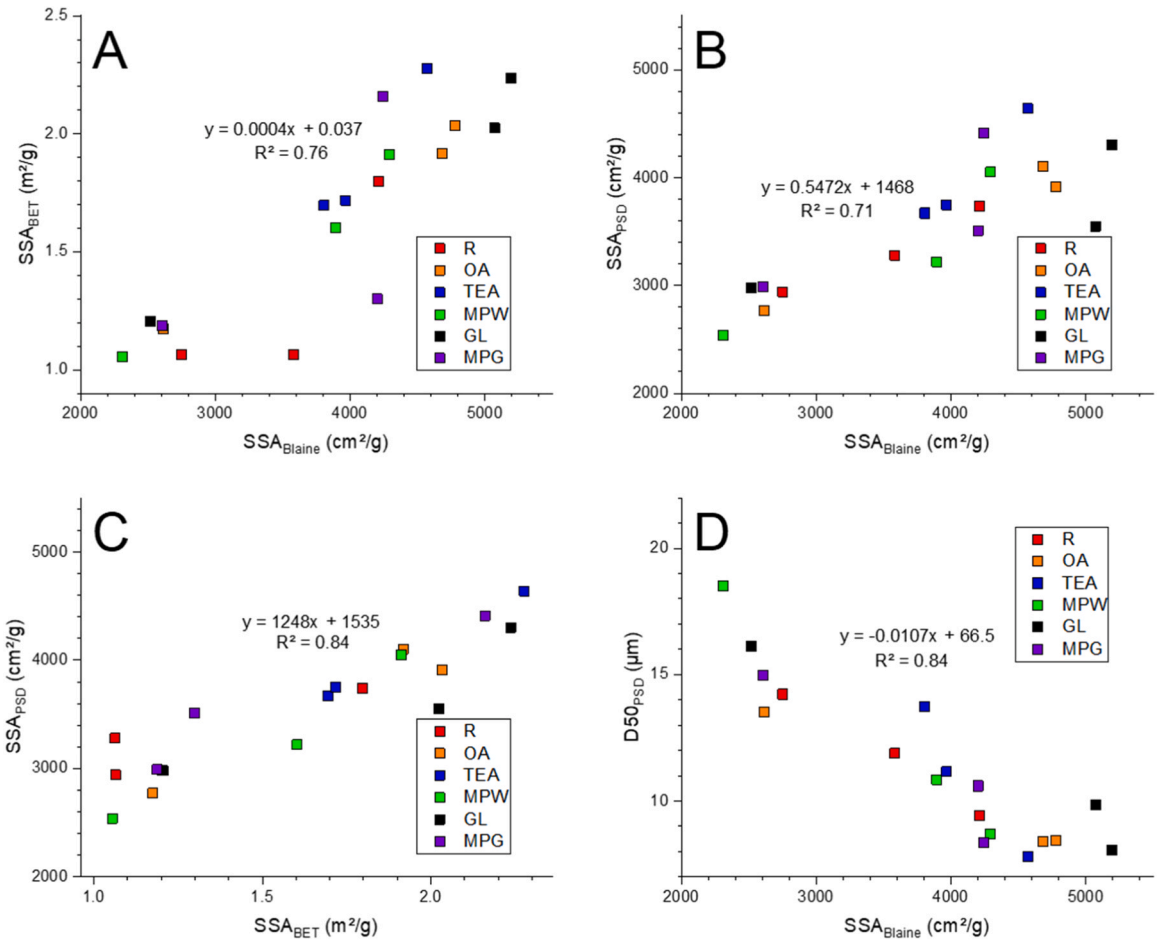

Fig. 1. Correlation between different measures of particle fineness. A) SSA_{Blaine} vs SSA_{BET}, B) SSA_{Blaine} vs SSA_{PSD}, C) SSA_{BET} vs SSA_{PSD} and D) SSA_{Blaine} vs $D50_{PSD}$.

differences between analytical principles used by each measuring technique, and their variation is consistent with data reported in literature [59,60]. Moreover, larger deviation between SSA_{Blaine}-SSA_{PSD} (Fig. 1 B) are present at higher SSA, meaning that at higher SSA these methods are more sensible to operator and sampling errors. After all, all methods seem to correlate with each other, aside from small amount of outliers. The correlation between the different methods suggests that each method could effectively be used to predict the reactivity of BOF slag if the reactivity of BOF slag correlates with the particle fineness. This statement is at least valid for the measured particle fineness ranges: i) D50 between 7.8 and 18.5 µm, ii) SSA_{PSD} between 2540 and 4640 cm^2/g iii) SSA_{Blaine} 2310–5190 cm^2/g and iv) SSA_{BET} 1.05–2.28 m^2/g. At higher or lower particle fineness it could be that a linear correlation no longer upholds and the correlation function becomes non-linear between different particle fineness methods. Moreover, due to theses correlations it seem irrelevant, which particle fineness measure is used to assess the reactivity in the following paragraphs. Due to the fact that in most research articles a D50 or a SSA_{Blaine} is reported, it is elected to focus more on these two particle fineness measures to assess the reactivity of BOF slag depending on particle fineness.

3.2. Isothermal calorimetry

Fig. 2 A and B present thermal power and cumulative heat curves of R samples (10, 20 and 30 min ground), respectively. R30 has the highest thermal power peak at ~1.8 mW/g after 12 hours. Shorter grinding times have the effect of delaying the hydration by almost doubling the induction periods from 5 hours to ~8 hours. More over the maximum of the thermal power curves of R10 and R20 are significantly lower than the one of R30 with maxima of 0.6 and 1.15 mW/g. The cumulative heat after 72 hours is lower for R10 and R20 than R30. R30 reaches ~95 J/g after 72 hours, where R10 and R20 reach 60 and 75 J/g, respectively. Hence, increasing the grinding times means increased reactivity early and higher heat generation in the early stages of hydration.

Fig. 2 C and D present the thermal power and cumulative heat curves of samples that were ground for 30 min. All samples that were ground with a grinding aid have a higher thermal power peak than R30. The highest thermal power peak which is also the earliest is the one of TEA30 (2.45 mW/g) reached 8 h after the start of hydration. TEA30 also generated the most cumulative heat after 72 hours of hydration (122 J/g). All other samples treated with a grinding aid have cumulative heat values after 72 h between TEA30 and R30 (95 J/g). Meaning that the addition of grinding aids will improve the reactivity of BOF slag (i.e. higher cumulative heat and higher thermal power maximum) at constant milling times. It should be noted that MPG30 is the only sample with grinding aid, in which the acceleratory period is slightly delayed. The acceleratory period of MPG30 is about 1 h layer compered to R30 and 3 h compared to MPG30, although MPG30 has a smaller D50 (8.3 µm) compared to R30 (13.5 µm) and a similar one compared to GL30 (8.1 µm). A potential explanation could be that the glycerol 1 M K3CitH promotes an initial complexation on the surface of the BOF slag powder of the added K3CitH in solution and therefore delays the initial hydration of the BOF slag. However, when the complexation is eventually broken up hydration catches up to the other samples. As MPG30 has a higher cumulative heat compared to R30 and GL30. Fig. 3 A - D present D50/SSA_{Blaine} vs the cumulative heat after 24 and 72 h, respectively, for this study and other studies that have reported D50

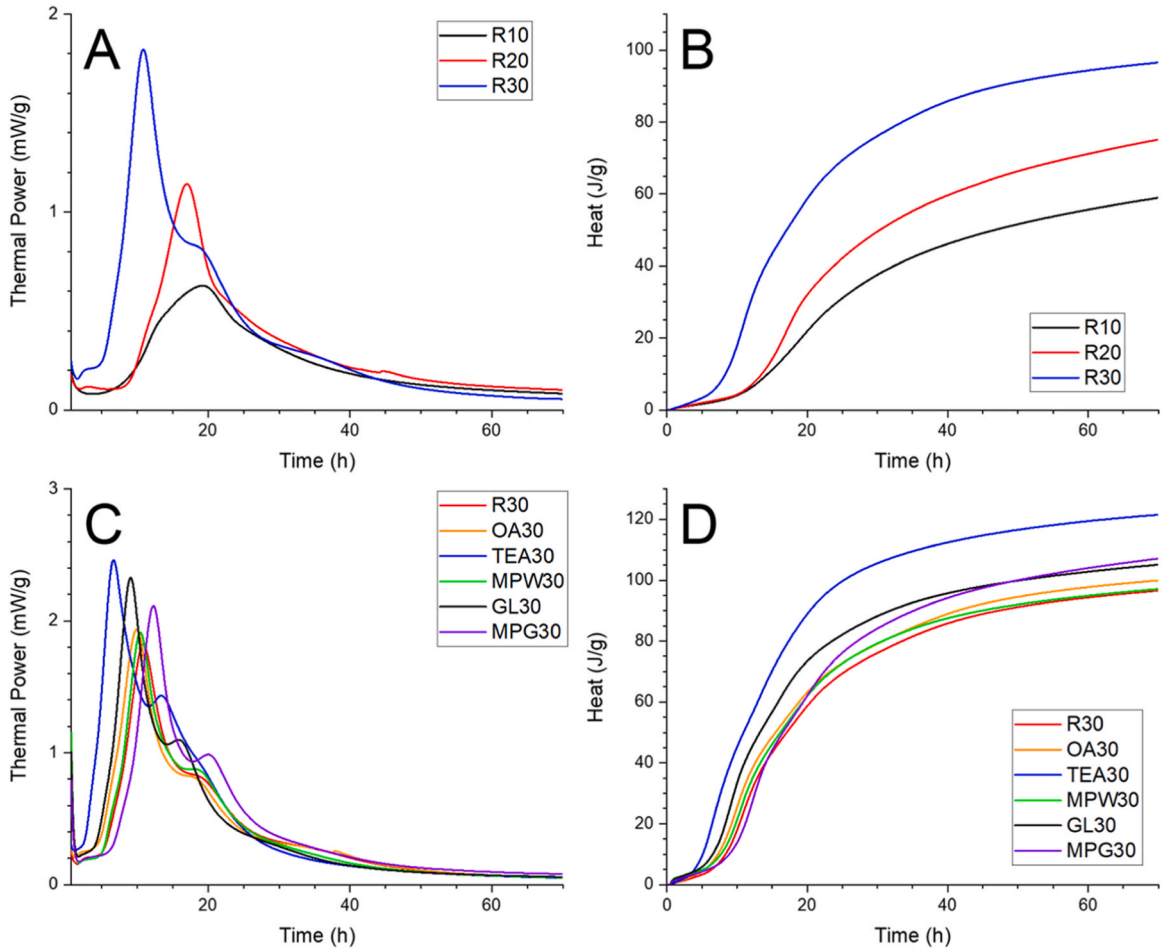

Fig. 2. A) Thermal power curves for the reference samples (R10, R20 and R30), B) cumulative heat curves for the reference samples, C) thermal power curves for 30 min milled samples and D) cumulative heat curves for 30 min milled samples.

and/or SSA_{Blaine} and isothermal calorimetry data. In general, high heat generation (> 70 J/g after 24 and 72 h) is absent in the presented data at high D50 (> 15 μm) and low SSA_{Blaine} (< 3500 cm^2/g). In contrast, cumulative heat is significantly higher after 72 h for all BOF slag data, if D50 is below < 10 μm and SSA_{Blaine} is above 4500 cm^2/g, except for non-activated BOF slag samples of [28].

It seems as OPC is less dependent on particle fineness compared to activated BOF slag. For example Sedaghat et al. [61] the D50 of an OPC is increased by milling from 14.4 to 5.2 μm which results in an increase of cumulative heat from 350 to 415 J/g (increase of ~18%) after 72 h, whereas the increase from R10 (D50 = 14.2 μm) to R30 (D50 = 9.4 μm) is 62% (60–97 J/g). The relatively higher cumulative heat increase for K3CitH activated BOF slag compared to OPC with higher particle fineness shows how important a high fineness is for K3CitH activated BOF slag to react with water. This is could be explained by the fact that the C_3S crystals of OPC dissolve more thoroughly and subsequently precipitate more hydration product independently from the particle fineness. More generally spoken, C_3S is more likely to dissolve completely by the hydration mechanism for which many theories exist, which are probably best summarized in [62]. In contrast, the dissolution of BOF slag initial phases are less. In K3CitH activated BOF slag, the most reactive phase $C_2(A,F)$ is: i) present in smaller amounts 15–25 wt% [24, 41] and ii) might react less thoroughly compared to C_3S in OPC. Hence, increasing the particle fineness and therefore the surface area that can react has a significantly higher effect on the reactivity of K3CitH activated BOF slag,

3.3. Thermographic analysis

Table 5 and Fig. 4 A – D report the results of TG and DTG analysis. When comparing the R10, R20 and R30 samples they show a significant difference in total mass loss from 5.2 wt% (R10) to 8.3 wt% (R30) after 7 days. However this difference becomes small as hydration proceeds (28 d) as the total mass loss of R10 increases to 7.2 wt% and the mass loss of R30 only to 8.4 wt%. The trend that longer milled samples do not show a significant increase in total mass loss between 7 and 28 days is also observed for the other 30 min milled samples with grinding aid. For example, the total mass loss for TEA30 and GL30 increases by 0.5 wt% and 0.8 wt% at 28 d, respectively.

Typical hydration products of BOF slag are hydrogarnet, pyroaurite, CSH and portlandite [31], which decompose between 40 – 500 °C. It should be noted that in K3CitH activated BOF slag, the phase assemblage of hydration products is similar only the hydration products may change relative to each other because C_2AF is more consumed during hydration and more hydrogranet is produced [24,41]. The mass loss in the temperature range between 40 – 180 °C is ranges from 1.8 to 4.2 wt% (7 day samples) and 2.7–4.5 wt% (28 day samples). In this temperature range, CSH dehydrates and pyroaurite usually or starts to dehydrate [24,39, 63]. In the temperature range between 180 – 410 °C pyroaurite further dehydrates and also hydrogarnet is known to dehydrate its bound water [31,39,64]. The significant mass loss in this temperature range (> 1 wt %) indicates that either one of these two phases has formed during hydration [24,31]. In contrary, all samples show only minor amount of mass loss in the typical temperature range of portlandite (410 – 500 °C) with a maximum of 0.6 wt% in TEA30.

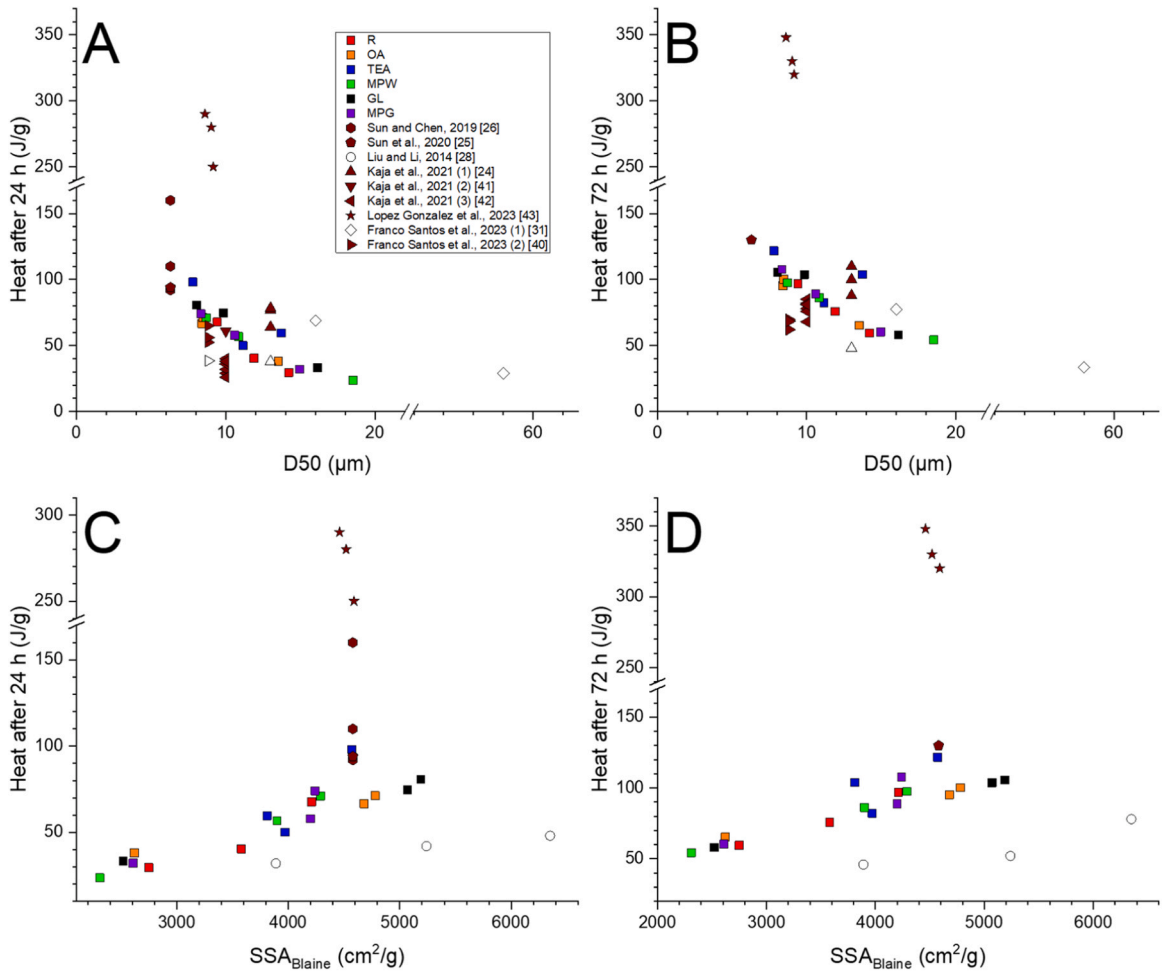

Fig. 3. Cumulative heat data of this study and data derived from the literature A) 24 h vs D50, B) 72 h vs D50, C) 24 h vs SSA$_{Blaine}$ and D) 72 h vs SSA$_{Blaine}$. It should be noted that in the literature data sometimes only one measure of particle fineness is reported or isothermal calorimetry measurement did not exceed 24 h, which explains the lack of all data points for the literature data. Non- activated BOF slag cumulative heat values are the empty symbols.

For a high amount of bound water (i.e. mass loss between 40 – 500 °C > 5 wt%) during the early hydration (first 7 days) high particle fineness plays an important role (Fig. 5 A) but less at later ages (Fig. 5 B). Moreover, high amounts of bound water correlate with higher strength [44]. High early strength of cementitious products is one of the most desired properties for the cement and concrete industry [65]. The relation between compressive strength is further discussed in Section 3.6.

3.4. Degree of reaction

The results of the RQPA are given in Table 6. The results of the RQPA for the IBOFS shows that the IBOFS material consists of four major phases C_2S (39.5 wt%), $C_2(A,F)$ (20 wt%), RO-Phase (25 wt%), which is a solid solution of FeO, MgO, MnO and CaO, and magnetite (Ff; 8.6 wt %). The results of the RQPA for IBOFS are in agreement with the results of the calculated values for C_2S, RO-Phase, Ff and and $C_2(A,F)$ based on the Bogue BOF slag approach [66]. Additionally, to the four major phases of BOF slag the typical weathering products of BOF slag, calcite (Cc) and portlandite [48] were present in small amounts (< 1 wt%).

All K3CitH activated hydrated samples at 7 and 28 days show the same phase assemblage with four major BOF slag phases still present and the presence of several hydration products. The hydration products that are present are portlandite (0.4 – 1.1 wt%), hydrogarnet (2.6 – 17.9 wt %), pyroaurite (3.3 – 8 wt%) and amorphous content (5 – 22.7 wt%). These hydration products are typical for the hydration of activated BOF slag and BOF slag hydrated in the presence of water [24,31,34,40,41]. However, their amounts and ratios may vary related to various factor such as the initial composition, particle fineness, pH and chemistry of the pore solution and duration of hydration. The four major BOF slag phases are consumed to a variable extend in all samples compared to IBOFS, but R10 at 7 days has still a high content of $C_2(A,F)$ (14.7 wt%) and C_2S (36.5 wt%), R30 has already a significantly lower amount of $C_2(A,F)$ (7.5 wt%) and C_2S (30.9 wt%). For TEA30 at 7 days the amounts of $C_2(A,F)$ and C_2S are even more reduced to 3.4 wt% and 26.1 wt%, respectively. The amounts of the four major BOF slag phases decreased for two reasons: i) the addition of chemically bound water to the hydrated BOF slag composition by itself causes a dilution of the four major BOF slag phases and ii) the effect of prime interest, the consumption of the four major BOF slag phases while participating in the hydration. In order to better see through the dilution effect and assess relative phase contributions to the hydration, the degree of hydration (DOH_j; i.e. fraction of reacted phase expressed as percentage) for each of the four major BOF slag phases (j) is calculate with Eq. 2:

$$DOH_j^t = 100 - \left(\frac{X_j^t * \left(\frac{100}{100 - X_{H_2O}^t}\right)}{X_j^0} * 100\right) \quad (2)$$

Whereas X_j^t is the amount of phase j in wt% (e.g. $C_2(A,F)$) determined by RQPA at the time t (e.g. 7 days), X_j^0 the amount of phase j in wt% before hydration in IBOFS determined by RQPA and $X_{H_2O}^t$ is the mass loss in wt

Table 5
Mass loss (wt%) of paste samples cured for 7 and 28 days in the various temperature ranges determined by TGA.

Mass loss (wt%) after **7 days** of hydration					
Temperature range	40–180 °C	180–410 °C	410–500 °C	40–500 °C	Total
R10	2.69	1.36	0.19	4.24	5.18
R20	3.46	2.64	0.34	6.44	7.64
R30	3.92	2.90	0.37	7.19	8.26
OA10	1.75	1.01	0.14	2.90	3.08
OA20	3.63	2.62	0.34	6.60	7.74
OA30	3.83	2.89	0.37	7.09	8.10
TEA10	3.68	3.27	0.42	7.37	8.78
TEA20	3.72	3.02	0.34	7.09	8.67
TEA30	4.10	3.78	0.47	8.36	10.06
MPW10	3.22	1.71	0.19	5.12	6.02
MPW20	3.56	2.91	0.37	6.84	8.06
MPW30	3.50	2.83	0.36	6.69	7.82
GL10	3.74	2.41	0.28	6.43	7.82
GL20	3.90	2.80	0.37	7.06	8.23
GL30	3.96	3.03	0.40	7.38	8.70
MPG10	3.27	1.50	0.23	5.00	6.03
MPG20	3.71	2.53	0.30	6.55	6.03
MPG30	4.23	3.05	0.39	7.67	9.06
Mass loss (wt%) after **28 days** of hydration					
Temperature range	40–180 °C	180–410 °C	410–500 °C	40–500 °C	Total
R10	3.72	2.08	0.29	6.09	7.20
R20	3.79	2.97	0.43	7.19	8.17
R30	3.86	3.07	0.45	7.38	8.41
OA10	2.67	1.59	0.19	4.44	5.23
OA20	3.92	3.01	0.43	7.36	8.59
OA30	4.22	3.32	0.51	8.05	9.31
TEA10	3.87	3.31	0.47	7.65	9.31
TEA20	4.18	3.46	0.50	8.15	9.49
TEA30	4.45	4.01	0.62	9.08	10.56
MPW10	4.26	2.53	0.35	7.13	8.51
MPW20	3.82	3.22	0.45	7.49	8.62
MPW30	4.11	3.32	0.49	7.93	9.12
GL10	3.90	2.70	0.36	6.96	7.92
GL20	4.23	3.34	0.52	8.09	9.24
GL30	4.36	3.39	0.53	8.27	9.49
MPG10	3.40	2.06	0.28	5.74	7.10
MPG20	4.05	3.25	0.45	7.75	9.18
MPG30	4.00	3.13	0.44	7.56	8.68

% between 40 – 500 °C determined by TGA at time t. Moreover, the total degree of hydration (TDOH) for each sample is calculated with Eq. 3:

$$TDOH^{t} = 100 - \left(\frac{X^{t}_{sum} * \left(\frac{100}{100 - X^{t}_{H_2O}} \right)}{X^{0}_{sum}} * 100 \right) \quad (3)$$

Whereas X^{t}_{sum} is the sum of RO-Phase, $C_2(A,F)$, C_2S and Ff in wt% at the time t, X^{0}_{sum} is the sum of RO-Phase, $C_2(A,F)$, C_2S and Ff in wt% in IBOFS and $X^{t}_{H_2O}$ is the mass loss in wt% between 40 – 500 °C determined by TGA at time t. The $TDOH^{t}$ expresses the total fraction (expressed as percentage) of the four major BOF slag phases that has participated in the hydration.

Table 7 gives the results for Eq. 1 and Eq. 2 after 7 and 28 days of hydration. The $DOH^{7days}_{C_2(A,F)}$ are the highest for all samples with an average of 58% and more than double than for each other initial phase. This observation confirms that $C_2(A,F)$ is the most reactive phase of K3CitH activated BOF slag of [24,41]. However, between 7 and 28 days the $C_2(A,F)$ does not react much more, as illustrated by the limited increase of $DOH^{28days}_{C_2(A,F)}$ (on average 61% for all samples) compared to $DOH^{7days}_{C_2(A,F)}$. In contrast, C_2S presents a higher increase from 7 to 28 days in their DOH. The DOH_{C_2S} increases by 7% from 18% to 25%. Also Ff and RO-Phase are participating in the first 7 days of hydration of K3CitH activated BOF slag as apparent from their average $DOH^{7days}_{RO-Phase}$ of 20% and DOH^{7days}_{Ff} of 18%. That the RO-Phase participates in the hydration of BOF slag has been reported earlier [22,31]. The participation of RO-Phase, Ff and C_2S in the hydration is highly dependent on the particle fineness, which is illustrated by the DOH of the samples R10, R20 and R30. For example the $DOH^{28days}_{C_2S}$ increases from 3% (R10) to 30% (R30). The fact that particle fineness is important to the early hydration (i.e. first 7 days) is also shown by the TDOH (Fig. 6 A). However, finer particle size (D50 < 14 μm) seems to become less important as the hydration progresses in time as samples with a D50 below 14 μm have a high $TDOH^{28\ days}$ above 30% (Fig. 6 B). Based on the TDOH and the amount of bound water that is lost between 40 – 500 °C (Fig. 6 A) it is concluded that K3CitH activated BOF slag is significantly more reactive (i.e. more initial phases dissolve and more water is bound during precipitation of hydrates) during the early hydration (7 days) if a D50 < 10 μm is achieved during milling.

3.5. Spread flow and compressive strength

Table 8 presents the results of the spread flow test, which is correlated with the particle fineness D50 in Fig. 7. Generally, lower D50 correlates with lower spread flow and therefore higher water demand for cementitious binders [67]. As grinding aids tend to improve the grindability of BOF slag [28,30], they increase particle fineness at similar milling times. For OPC it is known that a higher particle fineness (i.e. lower D50 or higher SSA) will decrease the spread flow [68] because of the higher water demand of particles below 8 μm, whereas larger particles above 24 μm have a lower water demand [67]. Almost all samples seem to follow the positive correlation between D50 and spread flow only OA10 and TEA10 deviate from this correlation.

Besides the results of the spread flow test Table 8 also reports the results of the compressive strength test on the pastes. Fig. 8 compares D50 with the compressive strength results at 7 and 28 days of this study and including some data from literature. Comparing the R10, R20 and R30 samples a significant increase in the 7 day compressive strength is observed with decreasing D50. The compressive strength increases from 19.7 (R10) to 35.2 MPa (R30) and after 28 days R30 has a compressive strength of 55.3 MPa. In Kaja et al. [24] the same w/b (0.16), activator and activator concentration was applied (sample C1 therein). Hence, this sample is more or less comparable to R10, R20 and R30. Sample C1 in [24] has a compressive strength of 36 MPa and 75 MPa at 7 days and 28 days, respectively. The strength value of this sample at 7 days is comparable to R30 but is significantly higher at 28 days (75 MPa for C1) although at a higher D50 (13 μm) compared to R30 (9.4 μm). Even though, the BOF slag from [24] is derived from the same steel plant, which means it has experienced the same processing procedure (i.e. cooling) it has a slightly different composition. More importantly, the BOF slag experienced a different material preparation (i.e. ball milling) than performed in this study (i.e. disk milling). The different milling of the BOF slag had the consequence that different particle size distribution curves are obtained. In [24], the BOF slag powder had a unimodal distribution, whereas particle size distribution curves in this study were all bimodal (not shown). So the slight difference in chemical composition and the different practices in raw material preparation have a significant influence on the mechanical properties. Especially it has an influence on the strength generation between 7 and 28 days. We prefer to argue that influence of different particle size distributions has a significantly higher effect on the mechanical properties than the slight difference in chemical composition. This argument is based on work on OPC where it has been shown that ideal packing of the binder fraction, which can be better achieved with an unimodal than with a bimodal particle size distribution, has a significant effect on the porosity and therefore on the development of mechanical strength [67–69]. It is therefore suggested that assessing and improving the packing of BOF slag powders is very important in order to achieve desirable higher mechanical strength of building products. An in-depth analysis of the packing is out of the scope

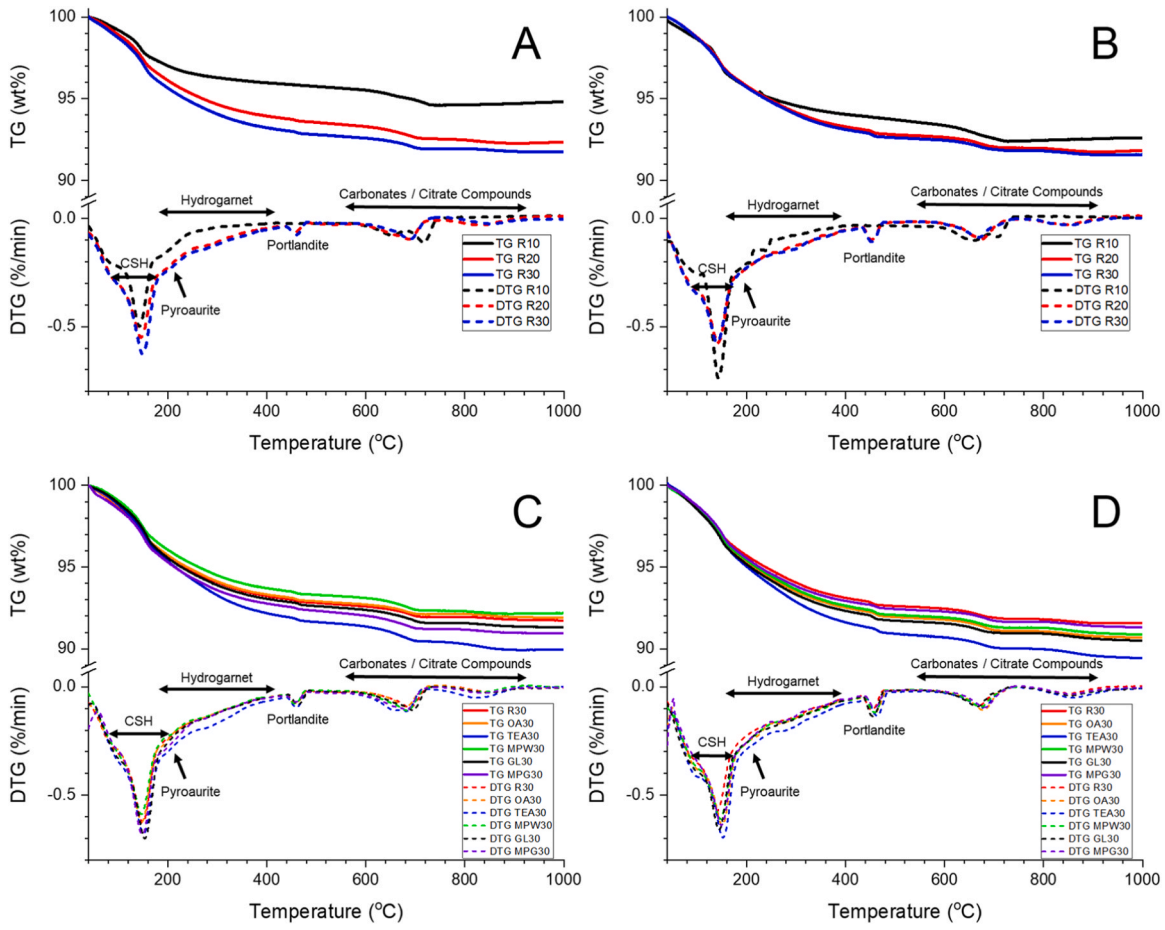

Fig. 4. TG and DTG curves of A) of the reference samples (R10, R20 and R30) after 7 days of hydration, B) of the reference samples (R10, R20 and R30) after 28 days of hydration, C) for 30 min milled samples after 7 days of hydration and D) for 30 min milled samples after 28 days of hydration.

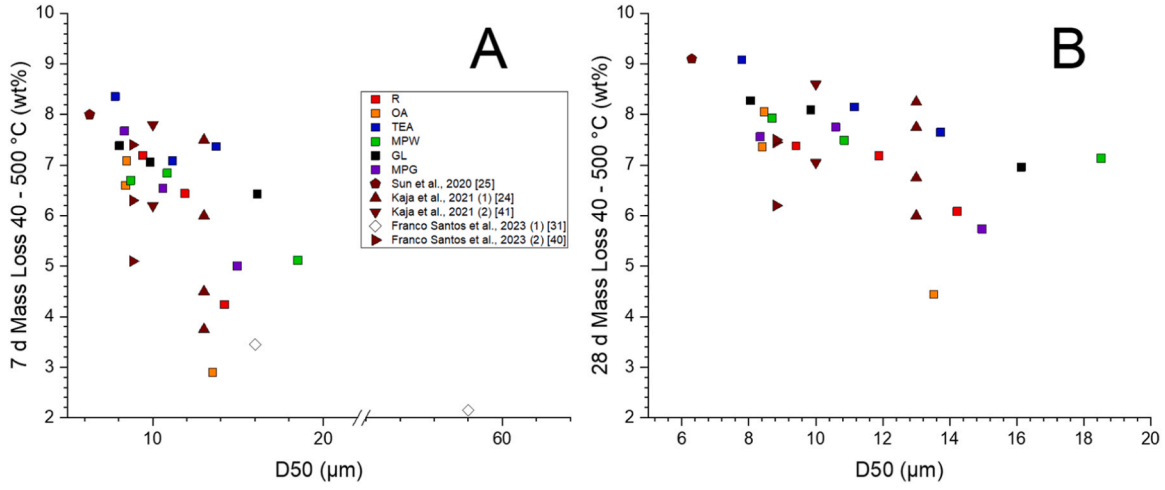

Fig. 5. Mass loss between 40 – 500 °C vs D50 of this study and data derived from the literature A) D50 vs 7 days mass loss between 40 – 500 °C and B) D50 vs 28 days mass loss between 40 – 500 °C.

of this study and is a future objective for research in order to enable the application of BOF slag stand-alone binders.

Samples that were prepared with a grinding aid mostly have higher compressive strength after 7 days. Highest compressive strength is achieved with MPG30 (70 MPa). The highest strength is achieved in MPG30 despite MPG30 not having the highest bound water content (i.e. mass loss between 40 – 500 °C) nor the highest $TDOH^{7\ d}$ (29%). This finding deviates from the general consensus that reaction degree correlates with strength and strength with particle fineness (D50; Fig. 8 A) in this study and perhaps should be attributed to better particle packing of MPG30. Also the other deviations from the correlation of compressive strength and particle fineness (D50; Fig. 8 A) may be explained in this way. After 28 days all 30 min samples milled with a grinding aid have higher strength than the reference sample (R30; 55.3 MPa). The

Table 6
Results of the RQPA (wt%) for the initial raw BOF slag (IBOFS), the calculated phase amounts for IBOFS based on the chemical composition in Table 2 according to the Bogue BOF slag approach [66], 7 and 28 days paste samples of K3CitH activated BOF slag.

		Raw Material		7 days hydration							
Phases	Cement Notation	$IBOFS^{RQPA}$	$IBOFS^{Bogue}$	R10	R20	R30	OA30	TEA30	MPW30	GL30	MPG30
RO-Phase	RO	25.0	22.2	23.2	18.9	17.1	18.4	17.0	18.4	18.0	19.1
Magnetite	Ff	8.6	9.3	8.1	7.0	6.7	6.2	5.8	6.6	5.9	6.2
Brownmilerite	$C_2(A,F)$	20.0	19.1	14.7	8.0	7.5	6.2	3.4	7.9	7.2	7.8
Belite	C_2S	39.5	44.2	36.5	30.4	30.9	29.8	26.1	30.2	28.3	28.1
Free Lime	C	0.6	2.1	0.8	0.9	0.7	0.7	0.4	0.5	0.3	0.2
Portlandite	CH	0.5	-	0.4	0.6	0.8	0.6	0.6	0.4	0.6	0.4
Calcite	Cc	0.4	-	0.2	0.3	0.2	0.2	0.3	0.3	0.3	0.3
Dolomite	(M,C)c	1.9	-	1.8	1.6	1.6	1.8	2.0	2.0	2.0	2.1
Hydrogarnet	$C_3(A,F)S_{3-x}H_{2x}$	0.0	-	2.6	9.8	10.0	8.7	14.2	8.6	9.6	8.8
Pyroaurite	$(M,f)_4(A,F)H_{10}$	0.0	-	3.3	6.0	6.1	8.0	6.8	5.8	7.4	7.2
Others	-	2.8	-	0.6	0.3	0.1	0.3	0.8	1.8	0.5	1.0
Amorphous	-	0.8	-	7.7	16.0	18.3	19.1	22.7	17.7	19.9	18.8
				28 days hydration							
Phases				R10	R20	R30	OA30	TEA30	MPW30	GL30	MPG30
RO-Phase	RO			21.6	15.6	16.5	16.6	16.1	18.0	19.5	17.6
Magnetite	Ff			6.7	6.4	6.5	6.6	6.2	6.8	6.1	6.5
Brownmilerite	$C_2(A,F)$			13.9	7.3	5.9	6.9	3.5	6.3	7.8	5.9
Belite	C_2S			36.1	26.1	25.5	26.7	24.4	27.4	25.3	27.1
Free Lime	C			0.4	0.2	0.2	0.3	0.1	0.3	0.4	0.5
Portlandite	CH			0.5	1.0	1.0	0.8	1.1	0.6	0.8	0.7
Calcite	Cc			0.1	0.6	0.4	0.3	0.7	0.5	0.3	0.2
Dolomite	(M,C)c			1.9	2.0	1.7	1.9	2.0	2.0	2.0	2.3
Hydrogarnet	$C_3(A,F)S_{3-x}H_{2x}$			3.5	12.2	13.3	12.1	17.9	12.4	12.4	12.0
Pyroaurite	$(M,f)_4(A,F)H_{10}$			4.8	6.2	6.2	6.2	7.1	6.4	5.6	7.9
Others	-			2.2	0.8	1.7	2.6	0.9	0.9	1.0	0.9
Amorphous	-			8.3	21.5	20.0	19.0	21.1	18.4	18.9	18.3

Table 7
Results of the DOH (%) calculation for each phase j and at time t (i.e. 7 or 28 days) calculated by Eq. 2. Results of TDOH (%) for each sample at time t (i.e. 7 or 28 days) calculated by Eq. 3.

	7 days							
Phase	R10	R20	R30	OA30	TEA30	MPW30	GL30	MPG30
RO	3.3	19.1	26.6	21.0	25.9	21.4	22.3	17.2
Ff	1.9	12.3	15.7	22.3	25.9	18.2	25.9	21.5
$C_2(A,F)$	23.1	57.1	59.6	66.5	81.3	57.7	61.1	57.6
C_2S	3.3	17.7	15.6	18.8	27.9	18.1	22.7	22.7
TDOH	7.4	26.1	28.0	30.0	38.7	27.5	31.1	28.6
	28 days							
Phase	R10	R20	R30	OA30	TEA30	MPW30	GL30	MPG30
RO	8.0	32.8	28.9	27.7	29.2	22.0	15.1	23.7
Ff	16.7	19.1	17.8	16.4	20.9	14.3	23.1	18.0
$C_2(A,F)$	26.1	60.5	68.3	62.5	80.6	65.9	57.4	67.9
C_2S	2.6	28.6	30.3	26.5	32.0	24.6	30.2	25.8
TDOH	10.4	35.7	36.9	33.6	40.7	31.8	31.3	33.5

maximum value is achieved by TEA30 with 78 MPa. This furthermore tells that particle fineness remains also very important at later ages (> 7 days) to achieve high strength (Fig. 8 B). How important it is for beyond 28 days still needs to be investigated. TEA30 appears to achieve the most optimal values showing the highest bound water content (9.1 wt%) and $TDOH^{28\ days}$ (40.7%). The strength of MPG30 decreased from 70 MPa (7 days) to 65 MPa (28 days), which is interpreted as fluctuation in material preparation. However, the achieved compressive strength of MPG30 after 28 days is still high (65 MPa).

In conclusion, BOF slag pastes activated with 1 wt% K3CitH can achieve high strength (> 50 MPa) already after 7 days. However, the particle fineness is required to be high (< 10 μm or > 4500 g/cm^2 SSA_{Blaine}) and w/b ratios need to be low (< 0.2). This is due to the generally lower water binding capacity compared to OPC in the early stage of the reaction. The low w/b makes the activated BOF slag binder difficult to control, and very susceptible to small differences in w/b ratio, particle fineness, potentially particle distribution curves, as borne out in a significant effects in the strength development of the activated BOF slag pastes. In addition, the low w/b ratio and high particle fineness has a negative effect on the flowability of BOF slag The usage of triethanolamine (TEA10, TEA20 and TEA30) seems to be the most favourable grinding aid in terms of achieving high compressive strength. That is because it not only produces high particle fineness but triethanolamine seem to have a positive effect on the hydration of BOF slag like it has for OPC or limestone calcined clay cements [38]. Particularly, triethanolamine may increase the hydration of $C_2(A,F)$ as it is reported for other alkanolamines in the literature [70,71].

3.6. Produced estimated CO_2 emissions for a BOF slag binder

Previously, it has been shown that BOF slag can be a viable alternative to save CO_2 emissions when applied as an SCM [72,73]. These studies showed that at 30 wt% of OPC replacement with BOF slag 25 – 30 wt% CO_2 emissions can be saved. However, this study aims for an OPC-free binder based on BOF slag, which would theoretically show even higher saving of CO_2 emissions. The estimation is calculated for TEA30, as this is the best performing sample. Here, a special case is presented for BOF slag applied as OPC-free binder in the Netherlands for

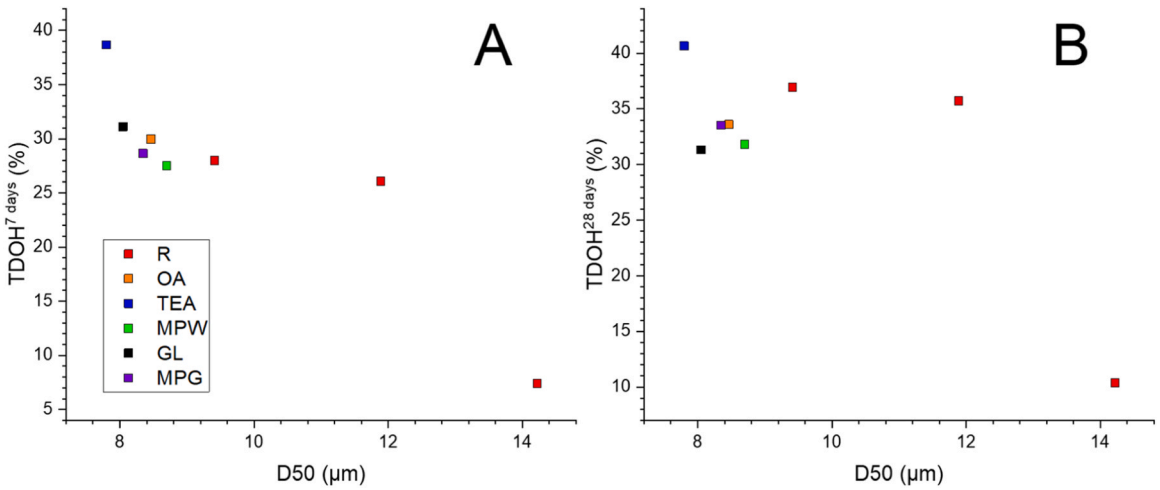

Fig. 6. TDOH vs D50 of this study A) D50 vs TDOH ^{7days} and B) D50 vs TDOH $^{28\ days}$.

Table 8
Results of spread flow and compressive strength tests of paste samples.

Sample	Spread Flow (cm)	Compr. Strength 7 days (MPa)	Compr. Strength 28 days (MPa)
R10	22.3	19.7	n.d.
R20	16.3	24.2	n.d.
R30	12.0	35.2	55.3
OA10	9.5	12.4	n.d.
OA20	9.5	35.1	n.d.
OA30	9.0	43.9	58.8
TEA10	12.8	43.0	n.d.
TEA20	14.5	32.8	n.d.
TEA30	9.5	60.6	78.0
MPW10	25.0	17.8	n.d.
MPW20	17.0	47.2	n.d.
MPW30	11.8	60.8	66.7
GL10	25.0	14.4	n.d.
GL20	9.8	44.3	n.d.
GL30	9.5	53.5	71.6
MPG10	25.0	23.1	n.d.
MPG20	12.0	51.7	n.d.
MPG30	11.0	69.9	64.8

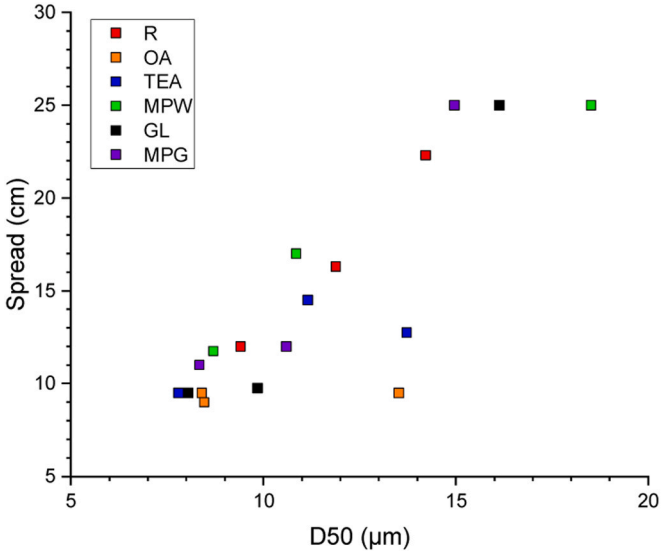

Fig. 7. D50 vs spread flow measurements.

two reasons. One reason is that the studied BOF slag is derived from the Tata Steel plant IJmuiden, which is located in the Netherlands. The second reason is that the Netherlands does not have an OPC clinker production site and all OPC clinker that is used for the production of cement is imported. Table 9 presents the key numbers that were used to calculate the CO_2 emissions per ton of BOF slag based binder in comparison to a common OPC. The Dutch Organization for Applied Scientific Research (TNO) published a report for decarburization options for the Dutch cement industry [74], which provided the best estimates for the emitted tCO_2/t OPC. The TNO report also provides the numbers for emitted tCO_2/t for drying the raw material and the electricity consumption required for grinding. The numbers that were used are from the ENCI IJmuiden cement grinding facility due to the close proximity to the Tata Steel plant IJmuiden. To calculate the emitted tCO_2/t for the BOF slag based binder the same numbers for drying and the electricity consumption of the grinding of blast furnace slag and the general cement production were used, respectively. The translation from grinding electricity consumption to emitted tCO_2/t were based on the specific CO_2 emissions in the Dutch electricity generation [75]. The emitted tCO_2/t for the K3CitH and the grinding aid TEA were taken from [76] and [77], respectively.

Table 10 presents the calculated emitted tCO_2/t of the BOF slag based binder compared to an OPC both produced in the Netherlands. The estimated emitted tCO_2/t of BOF slag based binder are only 7% of the OPC tCO_2/t, due to the absence of the clinkering process which is reported to be the main cause of emitted tCO_2/t of an OPC (~90%) [2]. Hence, the BOF slag based binder could potentially save large amounts of CO_2 emissions if applied in the Netherlands over OPC. However, the transition to mortar and concrete scale is still absent. Only two studies have been found in the literature that discuss the application of a BOF slag based binder on a mortar scale at increased binder over aggregate ratio [41,78]. An increased binder over aggregate ratio would always make the mortar or concrete products economically questionable, but obviously from CO_2 emission point of view still very advantageous.

4. Conclusions

This study presented an overview of the effects of five different grinding aids on the grindability of BOF slag and the resultant properties of BOF slag regrading particle fineness in relation to cementitious reactivity. It was possible to relate hydration properties such as heat release, bound water content, degree of hydration and mechanical properties to the particle fineness of the investigated BOF slag powders. The findings presented in this study are based on a multi analytical approach that combined particle fineness or specific surface area

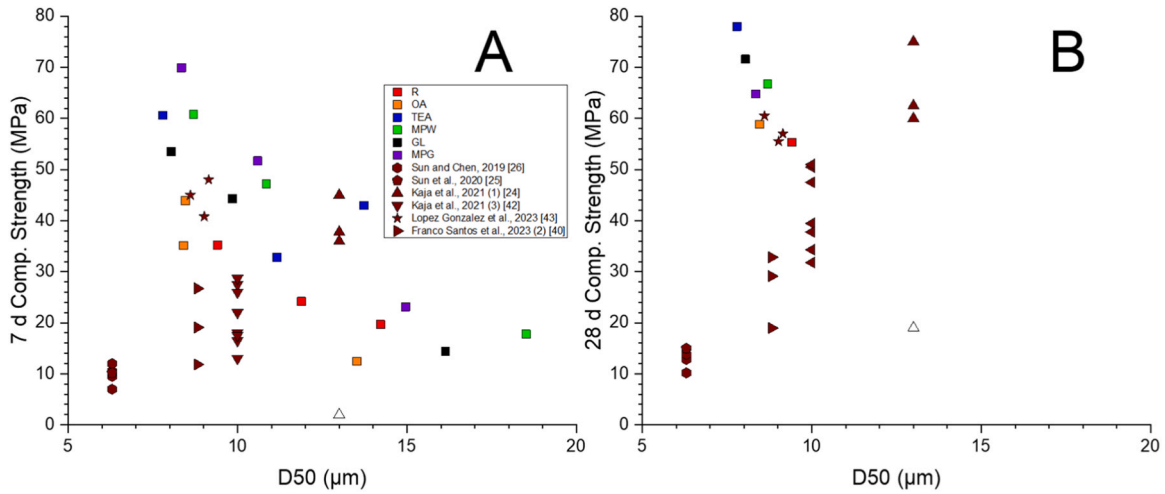

Fig. 8. Compressive strength vs D50 of this study and data derived from the literature A) D50 vs 7 days compressive strength and B) D50 vs 28 days compressive strength.

Table 9
Key numbers to calculate the estimated emitted CO_2 emissions of OPC and a BOF slag binder for Table 10.

Type	Number	Unit	Reference
OPC clinkering + transport	0.865889	tCO2/t	[74]
Drying	0.0196	tCO2/t	[74]
Electricity consumption grinding	72.02	kWh/t	[74]
CO_2 emission on electricity	0.000373	tCO_2/kWh	[75]
K3CitH	1.8	tCO2/t	[76]
TEA	0.705	tCO2/t	[77]

Table 10
Calculated emitted CO_2/t binder (i.e. OPC and BOF slag/TEA30).

Processing and Materials	OPC (tCO_2/t)	BOF slag (tCO_2/t)
clinkering + transport	0.8659	n.r.
Drying	n.r.	0.0196
Grinding	0.0269	0.0269
1 wt% K3CitH addition	n.r.	0.0180
0.05 wt% TEA addition	n.r.	0.0004
Total	0.8928	0.0648

Footnote: n.r. stands for not required.

analysis by LD-PSD, BET and Blaine method (EN 196–6), cementitious reactivity by isothermal calorimetry, bound water content analysis by TGA and degree of hydration determination by the combining RQPA results with TGA and compressive strength on past samples. Moreover, the data of this study was compared to data on BOF slag in literature in order to illustrate the importance of particle fineness of BOF slag for cementitious properties.

The findings of the study can be summarized as following:

- Prolonging the milling time has a significant influence on the cementitious properties of 1 wt% K3CitH activated BOF slag. However, it should be noted that the laboratory batch milling process with the particular milling equipment (i.e. disc mill) is not comparable with an industrial milling process.
- The studied grinding aids improve on average the grindability of BOF slag by 17%, which improve cementitious properties of 1 wt% K3CitH activated BOF slag.
- The used grinding aids change significantly the hydration phases that develop during the hydration, but rather enhance their formation.
- The reactivity of activated BOF slag appears more sensitive to particle fineness compared to OPC. A decrease in D50 from 14.2 µm to 9.4 µm is accompanied by an increase in the cumulative heat after 72 h by 62% (from 60 to 97 J/g).
- The usage of TEA as grinding aid is most favourable for the cementitious properties of 1 wt% K3CitH activated BOF slag, because the samples prepared with triethanolamine as grinding aid (TEA10, TEA20 and TEA30) achieve on average the highest heat after 24 (69 J/g) and 72 h (103 J/g), highest average bound water content after 7 (7.6 wt%) and 28 days (8.3 wt%) of hydration, on average second highest compressive strength values after 7 days of curing (45.5 MPa). The usage of triethanolamine seem to not only improve the grindability of BOF slag but also the hydration of BOF slag.
- The addition of literature data showed that K3CitH seems to be the most favourable activator for BOF slag in order to achieve high strength. Also, hot stage modification by the addition of Al_2O_3 in combination with wet granulation may be very favourable for the cementitious properties of BOF slag but might be a very cumbersome way of modifying BOF slag.
- Also it is unknown, which role plays the chemical composition, cooling history and the degree of weathering for the cementitious properties of BOF slag and whether their effects can be compensated by a certain activator or industrial milling procedure.
- At the end, an estimation for emitted tCO_2/t BOF slag binder was given and compared to common OPC, which showed that applying K3CitH activated BOF slag as binder instead of OPC could save up 93% of CO_2 emissions of a binder.

Future research outlook for BOF slag binders

Overall, to apply BOF slag as a stand-alone binder in a cementitious product requires still a lot of work. One point is to obtain the optimal particle fineness and hence cementitious properties of BOF slag with industrial scale milling. Moreover, data at mortar and concrete level experiments are vastly scarce in the literature for BOF slag or activated BOF slag. One important thing to highlight is that when moving to the mortar or concrete level one should always consider that BOF slag has a higher specific density (~3.6 g/cm^3) compared to OPC (~3.1 g/cm^3) [13,44]. Therefore an adjustment is required to have the same volume of binder compared to the aggregate and water in the mortar or concrete product as it was proposed in [44,45]. In a mortar or concrete purely based on BOF slag as a binder this would mean that the water to binder ratio (w/b) and binder over aggregate ratio (a/b) needs to be adjusted. For example if EN 196–1 is followed with a BOF slag based binder

(specific density of 3.6 g/cm^3) then 520 g of BOF slag binder should be used instead the 450 g according to the mass based standard, whereas amount of water and aggregate are kept the same.

Moreover, previous research also presented in this study focused exclusively on paste level investigations. This leads to the assumption that scientific laboratories are only milling on small scales 1 – 2 kg/h, which is very labour intensive to gain binder fine material for mortar and concrete level experiments. This was also one of the main limitations of this study. Therefore, it is advised that scientific labs should invest in larger milling installations, which could mill 50 – 100 kg/h. The investment in larger milling installations of course will also help to develop other alternative binders to further help with the decarburization of the cement industry. The transition to mortar and concrete level in the BOF slag based binder research will help to study the properties such as durability of developed products.

Declaration of Competing Interest

The authors declare that they have no known competing financial interests or personal relationships that could have appeared to influence the work reported in this paper.

Data Availability

Data will be made available on request.

Acknowledgments

The authors would like to appreciate the financial support of the Nederlandse Organisatie voor Wetenschappelijk Onderzoek (NWO) by funding this research (project no.10023338) and Materials Innovation Institute (M2i) for managing this project. Acknowledged is also the work of Mary Wijngaarden-Kroft of Tata Steel Netherlands, who helped with the sample preparation and analysing the XRD samples.

Appendix A. Supporting information

Supplementary data associated with this article can be found in the online version at doi:10.1016/j.jcou.2024.102821.

References

[1] F. Puertas, I. García-Díaz, A. Barba, M.F. Gazulla, M. Palacios, M.P. Gómez, et al., Ceramic wastes as alternative raw materials for Portland cement clinker production, Cem. Concr. Compos 30 (2008) 798–805, https://doi.org/10.1016/j.cemconcomp.2008.06.003.
[2] E. Benhelal, E. Shamsaei, M.I. Rashid, Challenges against CO2 abatement strategies in cement industry: a review, J. Environ. Sci. 104 (2021) 84–101, https://doi.org/10.1016/j.jes.2020.11.020.
[3] R. Snellings, P. Suraneni, J. Skibsted, Future and emerging supplementary cementitious materials, Cem. Concr. Res 171 (2023), https://doi.org/10.1016/j.cemconres.2023.107199.
[4] M.C.G. Juenger, F. Winnefeld, J.L. Provis, J.H. Ideker, Advances in alternative cementitious binders, Cem. Concr. Res 41 (2011) 1232–1243, https://doi.org/10.1016/j.cemconres.2010.11.012.
[5] M.C. Collivignarelli, A. Abbà, M. Carnevale Miino, G. Cillari, P. Ricciardi, A review on alternative binders, admixtures and water for the production of sustainable concrete, J. Clean. Prod. 295 (2021), https://doi.org/10.1016/j.jclepro.2021.126408.
[6] V.A. Nunes, P.H.R. Borges, Recent advances in the reuse of steel slags and future perspectives as binder and aggregate for alkali-activated materials, Constr. Build. Mater. 281 (2021) 122605, https://doi.org/10.1016/j.conbuildmat.2021.122605.
[7] L.M. Juckes, J. Grabowski, Transactions of the institutions of mining and metallurgy: section C The volume stability of modern steelmaking slags the volume stability of modern steelmaking slags. Min. Process Extr. Met. 112 (2003) 177–197, https://doi.org/10.1179/03719550322500370.
[8] H. Jalkanen, L. Holappa, Converter Steelmaking, vol. 3, in: S. Seetharaman, A. McLean, R. Guthrie, S. Sridhar (Eds.), Treatise Process Metall. Ind. Process., Elsevier Ltd, Oxford, 2014, pp. 223–270, https://doi.org/10.1016/B978-0-08-096988-6.00014-6. vol. 3.
[9] World Steel Association. Steel Statistical Yearbook 2020 Extended Version. Brussels, Belgium: 2020.
[10] J. Guo, Y. Bao, M. Wang, Steel slag in China: Treatment, recycling, and management, Waste Manag 78 (2018) 318–330, https://doi.org/10.1016/j.wasman.2018.04.045.
[11] H. Pöllmann. Industrial Waste, 1st ed, de Gruyter, Berlin, Germany, 2021, https://doi.org/10.1515/9783110674941.
[12] I.Z. Yildirim, M. Prezzi, Geotechnical Properties of Fresh and Aged Basic Oxygen Furnace Steel Slag, J. Mater. Civ. Eng. 27 (2015) 04015046, https://doi.org/10.1061/(asce)mt.1943-5533.0001310.
[13] A.C.P. Martins, J.M. Franco de Carvalho, L.C.B. Costa, H.D. Andrade, T.V. de Melo, J.C.L. Ribeiro, et al., Steel slags in cement-based composites: An ultimate review on characterization, applications and performance, Constr. Build. Mater. 291 (2021) 123265, https://doi.org/10.1016/j.conbuildmat.2021.123265.
[14] Q. Wang, P. Yan, J. Yang, B. Zhang, Influence of steel slag on mechanical properties and durability of concrete, Constr. Build. Mater. 47 (2013) 1414–1420, https://doi.org/10.1016/j.conbuildmat.2013.06.044.
[15] Y. Jiang, T.C. Ling, C. Shi, S.Y. Pan, Characteristics of steel slags and their use in cement and concrete—A review, Resour. Conserv Recycl 136 (2018) 187–197, https://doi.org/10.1016/j.resconrec.2018.04.023.
[16] K. Schraut, B. Adamczyk, C. Adam, D. Stephan, B. Meng, S. Simon, et al., Cement and Concrete Research Synthesis and characterisation of alites from reduced basic oxygen furnace slags, Cem. Concr. Res 147 (2021), https://doi.org/10.1016/j.cemconres.2021.106518 (Received.).
[17] Hewlett, P.C. Liska, M. Aïtcin, P.-C. Beaudoin, J.J. Bensted, J. van Deventer JSJ, et al.. Lea" s Chemistry of Cement and Concrete, 5th ed, Butterworth-Heinemann, Oxford, 2019 vol. 58.
[18] J.N. Murphy, T.R. Meadowcroft, R. de Assis Moreira, P.V. Barr, Enhancement of the cementitious properties of steelmaking slag, Can. Met. Q 36 (1997) 315–331, https://doi.org/10.1179/cmq.1997.36.5.315.
[19] E. Belhadj, C. Diliberto, A. Lecomte, Characterization and activation of Basic Oxygen Furnace slag, Cem. Concr. Compos 34 (2012) 34–40, https://doi.org/10.1016/j.cemconcomp.2011.08.012.
[20] S. Zhuang, Q. Wang, Inhibition mechanisms of steel slag on the early-age hydration of cement, Cem. Concr. Res 140 (2021), https://doi.org/10.1016/j.cemconres.2020.106283.
[21] L. Chen, H. Wang, K. Zheng, J. Zhou, F. He, Q. Yuan, The mechanism of basic oxygen furnace steel slag retarding early-age hydration of Portland cement and mitigating approach towards higher utilization rate, J. Clean. Prod. 362 (2022) 132493, https://doi.org/10.1016/j.jclepro.2022.132493.
[22] J.C.O. Zepper, S.R. van der Laan, K. Schollbach, H.J.H. Brouwers, Reactivity of BOF slag under autoclaving conditions, Constr. Build. Mater. 364 (2023), https://doi.org/10.1016/j.conbuildmat.2022.129957.
[23] E. Belhadj, C. Diliberto, A. Lecomte, Properties of hydraulic paste of basic oxygen furnace slag, Cem. Concr. Compos 45 (2014) 15–21, https://doi.org/10.1016/j.cemconcomp.2013.09.016.
[24] A.M. Kaja, K. Schollbach, S. Melzer, S.R. van der Laan, H.J.H. Brouwers, Q. Yu, Hydration of potassium citrate-activated BOF slag, Cem. Concr. Res 140 (2021) 1–11, https://doi.org/10.1016/j.cemconres.2020.106291.
[25] J. Sun, Z. Zhang, S. Zhuang, W. He, Hydration properties and microstructure characteristics of alkali – activated steel slag, Constr. Build. Mater. 241 (2020) 118–141, https://doi.org/10.1016/j.conbuildmat.2020.118141.
[26] J. Sun, Z. Chen, Effect of silicate modulus of water glass on the hydration of alkali-activated converter steel slag, J. Therm. Anal. Calor. 138 (2019) 47–56, https://doi.org/10.1007/s10973-019-08146-3.
[27] D. Wang, J. Chang, W.S. Ansari, The effects of carbonation and hydration on the mineralogy and microstructure of basic oxygen furnace slag products, J. CO2 Util. 34 (2019) 87–98, https://doi.org/10.1016/j.jcou.2019.06.001.
[28] S. Liu, L. Li, Influence of fineness on the cementitious properties of steel slag, J. Therm. Anal. Calor. 117 (2014) 629–634, https://doi.org/10.1007/s10973-014-3789-0.
[29] B. Huo, Y. Luo, B. Li, C. Chen, Y. Zhang, Influence of particle size on the reactivity of chemical modified steel slag powder, J. Sustain Cem. Mater. 12 (2023) 62–70, https://doi.org/10.1080/21650373.2021.2014368.
[30] X. Zhu, H. Hou, X. Huang, M. Zhou, W. Wang, Enhance hydration properties of steel slag using grinding aids by mechanochemical effect, Constr. Build. Mater. 29 (2012) 476–481, https://doi.org/10.1016/j.conbuildmat.2011.10.064.
[31] Franco Santos, W. Schollbach, K. Melzer, S. Laan, S.R. Van Der, H.J.H. Brouwers, Quantitative analysis and phase assemblage of basic oxygen furnace slag hydration, J. Hazard Mater. 450 (2023), https://doi.org/10.1016/j.jhazmat.2023.131029.
[32] J.J. Thomas, S. Ghazizadeh, E. Masoero, Kinetic mechanisms and activation energies for hydration of standard and highly reactive forms of β-dicalcium silicate (C2S), Cem. Concr. Res 100 (2017) 322–328, https://doi.org/10.1016/j.cemconres.2017.06.001.
[33] S. Wunderlich, T. Schirmer, U.E.A. Fittschen, Investigation on vanadium chemistry in basic-oxygen-furnace (BOF) slags—a first approach, Metals 11 (2021) 1–15, https://doi.org/10.3390/met11111869.
[34] P.Y. Mahieux, J.E. Aubert, G. Escadeillas, M. Measson, Quantification of hydraulic phase contained in a basic oxygen furnace slag, J. Mater. Civ. Eng. 26 (2014) 593–598, https://doi.org/10.1061/(asce)mt.1943-5533.0000867.
[35] S.K. Singh, Jyoti, P. Vashistha, Development of newer composite cement through mechano-chemical activation of steel slag, Constr. Build. Mater. 268 (2021) 121147, https://doi.org/10.1016/j.conbuildmat.2020.121147.
[36] J. Li, W. Ni, X. Wang, S. Zhu, X. Wei, F. Jiang, et al., Mechanical activation of medium basicity steel slag under dry condition for carbonation curing, J. Build. Eng. 50 (2022) 104123, https://doi.org/10.1016/j.jobe.2022.104123.

[37] P. Przwara, S. Breitung-Faes, A. Kwade, Impact of grinding aids on dry grinding performance, bulk properties and surface energy, Adv. Powder Technol. 29 (2018) 416–425, https://doi.org/10.1016/j.apt.2017.11.029.
[38] F. Zunino, K. Scrivener, Assessing the effect of alkanolamine grinding aids in limestone calcined clay cements hydration, Constr. Build. Mater. 266 (2021) 121293, https://doi.org/10.1016/j.conbuildmat.2020.121293.
[39] K. Scrivener, R. Snellings, B. Lothenbach, A Practical Guide to Microstructural Analysis of Cementitious Materials, CRC Press, Boca Raton, FL, United States, 2016, https://doi.org/10.1201/b19074.
[40] W. Franco Santos, J.J. Botterweg, S. Chaves Figueiredo, K. Schollbach, S. van der Laan, H.J.H. Brouwers, Sodium oxalate activation of basic oxygen furnace slag for building materials, Resour. Conserv Recycl 198 (2023) 107174, https://doi.org/10.1016/j.resconrec.2023.107174.
[41] A.M. Kaja, S. Melzer, H.J.H. Brouwers, Q. Yu, On the optimization of BOF slag hydration kinetics, Cem. Concr. Compos 124 (2021) 104262, https://doi.org/10.1016/j.cemconcomp.2021.104262.
[42] A.M. Kaja, A. Delsing, S.R. van der Laan, H.J.H. Brouwers, Q. Yu, Effects of carbonation on the retention of heavy metals in chemically activated BOF slag pastes, Cem. Concr. Res 148 (2021) 106534, https://doi.org/10.1016/j.cemconres.2021.106534.
[43] P.L. Lopez Gonzalez, R.M. Novais, J. Labrincha, B. Blanpain, Y. Pontikes, The impact of granulation on the mineralogy of a modified-BOF slag and the effect on kinetics and compressive strength after alkali activation, Cem. Concr. Compos 140 (2023) 105038, https://doi.org/10.1016/j.cemconcomp.2023.105038.
[44] M.J. Ahmed, W.F. Santos, H.J.H. Brouwers, Air granulated basic Oxygen furnace (BOF) slag application as a binder: Effect on strength, volumetric stability, hydration study, and environmental risk, Constr. Build. Mater. 367 (2023), https://doi.org/10.1016/j.conbuildmat.2023.130342.
[45] M.J. Ahmed, S. Durand, M. Antoun, F. Gauvin, S. Amziane, H.J.H. Brouwers, Utilization of air granulated basic oxygen furnace slag as a binder in belite calcium sulfoaluminate cement: a sustainable alternative, J. Clean. Prod. 436 (2024), https://doi.org/10.1016/j.jclepro.2023.140539.
[46] J. Zhao, Z. Li, D. Wang, P. Yan, L. Luo, H. Zhang, et al., Hydration superposition effect and mechanism of steel slag powder and granulated blast furnace slag powder, Constr. Build. Mater. 366 (2023) 130101, https://doi.org/10.1016/j.conbuildmat.2022.130101.
[47] Y. Zhao, T. Shi, L. Cao, L. Kan, M. Wu, Influence of steel slag on the properties of alkali-activated fly ash and blast-furnace slag based fiber reinforced composites, Cem. Concr. Compos 116 (2021) 103875, https://doi.org/10.1016/j.cemconcomp.2020.103875.
[48] Schollbach K., Laan S.Van Der. Long term weathering of converter slag. ICSBM 2019 – 2nd Int. Conf. Sustain. Build. Mater., 2019, p. 1–10.
[49] M. Tossavainen, F. Engstrom, Q. Yang, N. Menad, Characteristics of steel slag under different cooling conditions, Waste Manag 27 (2007) 1335–1344, https://doi.org/10.1016/j.wasman.2006.08.002.
[50] F. Engström, D. Adolfsson, Q. Yang, C. Samuelsson, B. Bjo, Crystallization behaviour of some steelmaking slags, Steel Res Int 81 (2010), https://doi.org/10.1002/srin.200900154.
[51] K. Schollbach, M.J. Ahmed, S.R. van der Laan, The mineralogy of air granulated converter slag, Int J. Ceram. Eng. Sci. (2020) 1–16, https://doi.org/10.1002/ces2.10074.
[52] P. Przwara, A. Kwade, Grinding aids for dry fine grinding processes – Part I: mechanism of action and lab-scale grinding, Powder Technol. 375 (2020) 146–160, https://doi.org/10.1016/j.powtec.2020.07.038.
[53] Y.M. Zhang, T.J. Napier-Munn, Effects of particle size distribution, surface area and chemical composition on Portland cement strength, Powder Technol. 83 (1995) 245–252, https://doi.org/10.1016/0032-5910(94)02964-P.
[54] I.B. Celik, The effects of particle size distribution and surface area upon cement strength development, Powder Technol. 188 (2009) 272–276, https://doi.org/10.1016/j.powtec.2008.05.007.
[55] M. Ibrahim, M. Maslehuddin, An overview of factors influencing the properties of alkali-activated binders, J. Clean. Prod. 286 (2021) 124972, https://doi.org/10.1016/j.jclepro.2020.124972.
[56] E.C. Arvaniti, M.C.G. Juenger, S.A. Bernal, J. Duchesne, L. Courard, S. Leroy, et al., Determination of particle size, surface area, and shape of supplementary cementitious materials by different techniques, Mater. Struct. Constr. 48 (2015) 3687–3701, https://doi.org/10.1617/s11527-014-0431-3.
[57] E.C. Arvaniti, M.C.G. Juenger, S.A. Bernal, J. Duchesne, L. Courard, S. Leroy, et al., Physical characterization methods for supplementary cementitious materials, Mater. Struct. Constr. 48 (2015) 3675–3686, https://doi.org/10.1617/s11527-014-0430-4.
[58] K. Sobolev, M.F. Gutiérrez, How nanotechnology can change the concrete world, Am. Ceram. Soc. Bull. 84 (2005) 14–18, https://doi.org/10.1002/9780470588260.ch17.
[59] C. Ferraris, E. Garboczi, Identifying improved standardized tests for measuring cement particle size and surface area, Transp. Res Rec. (2013) 10–16, https://doi.org/10.3141/2342-02.
[60] S. Mantellato, M. Palacios, R.J. Flatt, Reliable specific surface area measurements on anhydrous cements, Cem. Concr. Res 67 (2015) 286–291, https://doi.org/10.1016/j.cemconres.2014.10.009.
[61] A. Sedaghat, N. Shanahan, A. Zayed, Predicting one-day, three-day, and seven-day heat of hydration of Portland cement, J. Mater. Civ. Eng. 27 (2015) 1–12, https://doi.org/10.1061/(asce)mt.1943-5533.0001220.
[62] John E. The Effect of Artificial Calcium Silicate Hydrate on Cement Hydration. TU Berlin, 2022. https://doi.org/10.14279/depositonce-14882.
[63] V. Vágvölgyi, S.J. Palmer, J. Kristóf, N. Vidić, R.L. Frost, E. Horváth, Mechanism for hydrotalcite decomposition: A controlled rate thermal analysis study, J. Colloid Interface Sci. 318 (2008) 302–308, https://doi.org/10.1016/j.jcis.2007.10.033.
[64] Q. Shu, G.P. Brey, Ancient mantle metasomatism recorded in subcalcic garnet xenocrysts: temporal links between mantle metasomatism, diamond growth and crustal tectonomagmatism, Earth Planet Sci. Lett. 418 (2015) 27–39, https://doi.org/10.1016/j.epsl.2015.02.038.
[65] C.K.Y. Leung, T. Pheeraphan, Very high early strength of microwave cured concrete, Cem. Concr. Res 25 (1995) 136–146, https://doi.org/10.1016/0008-8846(94)00121-E.
[66] J.C.O. Zepper, S.R. van der Laan, K. Schollbach, H.J.H. Brouwers, A Bogue approach applied to basic oxygen furnace slag, Cem. Concr. Res 175 (2024) 107344, https://doi.org/10.1016/j.cemconres.2023.107344.
[67] T. Zhang, Q. Yu, J. Wei, P. Zhang, Effects of size fraction on composition and fundamental properties of Portland cement, Constr. Build. Mater. 25 (2011) 3038–3043, https://doi.org/10.1016/j.conbuildmat.2011.01.005.
[68] I. Mehdipour, K.H. Khayat, Effect of particle-size distribution and specific surface area of different binder systems on packing density and flow characteristics of cement paste, Elsevier Ltd (2017), https://doi.org/10.1016/j.cemconcomp.2017.01.005.
[69] W. Aiqin, Z. Chengzhi, Z. Ningsheng, Theoretic analysis of the influence of the particle size distribution of cement system on the property of cement, Cem. Concr. Res 29 (1999) 1721–1726, https://doi.org/10.1016/S0008-8846(99)00148-9.
[70] H. Kang, S. Kim, Y. Lee, S. Jung, J. Moon, Mechanochemical effect of alkanolamines on the C4AF: Crystal structure, hydration behavior, and strength enhancement, Cem. Concr. Compos 145 (2024) 105326, https://doi.org/10.1016/j.cemconcomp.2023.105326.
[71] H. Kang, S. Jung, J. Jung, J. Park, J.B. Park, J. Moon, Investigation of the effect of diethanol isopropanolamine on ferrite phase, J. Sustain Cem. Mater. 12 (2023) 1604–1616, https://doi.org/10.1080/21650373.2023.2248487.
[72] X. Gu, H. Wang, J. Liu, Z. Zhu, S. Wang, X. Xu, Synergistic effects of steel slag and metakaolin in cementitious systems: Packing properties, strength, and microstructure, Constr. Build. Mater. 411 (2024) 134395, https://doi.org/10.1016/j.conbuildmat.2023.134395.
[73] X. Sun, J. Liu, Y. Zhao, J. Zhao, Z. Li, Y. Sun, et al., Mechanical activation of steel slag to prepare supplementary cementitious materials: A comparative research based on the particle size distribution, hydration, toxicity assessment and carbon dioxide emission, J. Build. Eng. 60 (2022) 105200, https://doi.org/10.1016/j.jobe.2022.105200.
[74] C. Xavier, C. Oliveira, Decarbonisation options for the Dutch Cement INdustry, The Hague, The Netherlands, 2021.
[75] P. Silva Ortiz, D. Flórez-Orrego, S. de Oliveira Junior, R. Maciel Filho, P. Osseweijer, J. Posada, Unit exergy cost and specific CO2 emissions of the electricity generation in the Netherlands, Energy 208 (2020), https://doi.org/10.1016/j.energy.2020.118279.
[76] Q. Huang, Z. Tao, Z. Pan, R. Wuhrer, M. Rahme, Use of sodium/potassium citrate to enhance strength development in carbonate-activated hybrid cement, Constr. Build. Mater. 350 (2022) 128913, https://doi.org/10.1016/j.conbuildmat.2022.128913.
[77] Azapagic A., Amienyo D., Cuéllar Franca R.M., Jeswani H.K. Carbon Footprints of Recycled Solvents Study for the European Solvent Recycler Group. Manchester, UK: 2013.
[78] Z. Jiang, J. Zepper, X. Ling, K. Schollbach, H.J.H. Brouwers, Potassium citrate-activated pure BOF slag-based mortars utilizing carbonated and autoclaved BOF slag aggregates, Cem. Concr. Compos 150 (2024) 105564, https://doi.org/10.1016/j.cemconcomp.2024.105564.